International Journal of Heat and Mass Transfer 128 (2019) 115–124

Contents lists available at ScienceDirect

International Journal of Heat and Mass Transfer

journal homepage: www.elsevier.com/locate/ijhmt

Drop evaporation of hydrocarbon fluids with deposit formation

Philipp Hänichen *, Achim Bender, Bernhard Voß, Tatiana Gambaryan-Roisman, Peter Stephan

Institute for Technical Thermodynamics, Technische Universität Darmstadt, Alarich-Weiss-Straße 10, 64287 Darmstadt, Germany

ARTICLE INFO

Article history:
Received 15 November 2017
Received in revised form 22 August 2018
Accepted 23 August 2018
Available online 4 September 2018

Keywords:
Deposit formation
Phase change
Heat transfer
Drop evaporation
Contact angle measurements

ABSTRACT

The evaporation and deposit formation process of a hydrocarbon drop on a heated aluminium surface is experimentally investigated and compared to a physico-mathematical model. To analyze the effect of wall temperature on deposit formation, the experiments are conducted for three substrate temperatures below, one temperature close to and one temperature above the saturation point for atmospheric pressure. In each experimental run 500 single drops with constant volume are deposited and evaporated successively. The shape evolution of the drops is recorded with a monochrome camera sidewards. The deposited mass is evaluated as well as the contact angle evolution and drop lifetime. The experiments show a strong dependency of the contact angle on the deposit formation and on the wall temperature. With higher wall temperatures and an ongoing deposit formation, the initial contact angles increase and drop lifetime is reduced. The appearing deposits vary from light yellow and highly viscous films to dark brown solid layers and black particles, depending on the applied substrate temperatures. The model based calculations show a possibility to describe the evaporation process with effective diffusive transport.

1. Introduction

Evaporating fuel compounds on hot internal walls of automotive combustion engines tend to form deposits leading to increased NO_x and particulate emissions, misfire and reduced engine torque. The liquid hydrocarbons undergo various oxidative reactions and polymerization. This complex deposit formation process interacts strongly with the hydrodynamics and heat transport. Porous deposit layers are preferentially wetted and the liquid phase can be trapped inside cavities. During evaporation, low boiling fractions evaporate whereas the compounds with higher saturation temperatures remain on the walls. The local deposit layers lead to an uneven heat transfer through the wall. Depending on deposit morphology, roughness and porosity, the heat transfer and, thus, evaporation rate and deposit growth are influenced. A basic insight in the local evaporation phenomena is required to understand the mechanisms of the deposit formation.

In literature numerous engine dynamometer experiments are reported, in which the global impacts of fuel derived deposits on engine performance or the effect of operating conditions and different fuels on deposit growth are investigated. Arters et al. [1] found injector fouling to be correlated with fuel consumption, hydrocarbon and carbon monoxide emissions, as well as particulate emissions.

Generally, the deposit formation is stronger in direct injection gasoline engines than in port fuel injection engines [2]. Güralp et al. [3] conducted engine dynamometer tests with a homogeneous charge compression ignition test engine and concluded that the effect of combustion chamber deposits on bulk burning near the wall is greater than the global reduction of heat loss. As shown by Kinoshita et al. [4], injector nozzle temperatures above the fuel's T90 temperature lead to increased deposit formation as deposit precursors remain on the nozzle surface after a dryout. With an Electron Probe Micro Analysis of the deposits, the authors proved aromatic compounds to be one of the major functional groups of the deposits. Similar observations have been done by Ashida et al. [5], who also stated that the alkyl substituents influence the formation of injector deposits.

Recently numerous experimental investigations on a laboratory scale have been performed. Richter et al. [6] conducted a 70-h long-term experiment, in which Diesel fuel probes were heated up to 110 °C and 150 °C. The authors detected oxidized aromatic compounds, which are thought to be responsible for the carbon based deposit layers on injector components. Song et al. [7] investigated the effects of deposits on spray behavior of a gasoline direct injector. The coral shaped deposits with particle sizes of less than 5 µm lead to an increased spray cone angle and to a decrease of the spray particle size in combination with a higher standard

* Corresponding author.
E-mail address: haenichen@ttd.tu-darmstadt.de (P. Hänichen).

https://doi.org/10.1016/j.ijheatmasstransfer.2018.08.102
0017-9310/

deviation. Generic experiments have been done by Arifin et al. [8,9], who investigated the deposit formation of single diesel and bio-diesel drops impinging and evaporating on a hot plate. Deegan et al. [10] firstly reported of capillary flows inside sessile drops carrying dispersed solid particles from the bulk to the edge region. The resulting ring deposits are often referred to as the coffee stains. As liquid evaporates mainly at the triple line, particles accumulate in that region. Similar deposit phenomena are observed for evaporating solutions. Due to the high local heatflux, the saturation concentration is reached initially at the triple line and solutes mainly precipitate or crystallize close to the edge of sessile drops. Schmid et al. [11] investigated this crystallization process for evaporating urea-water drops on heated surfaces and observed a significant heat release when the urea concentration reached the supersaturated conditions at the triple line. Drops evaporating on heated walls without deposit formation have been investigated by various authors. Crafton and Black [12] investigated experimentally evaporation of water and *n*-heptane droplets on copper and aluminum substrates. They found that the evolution of diameter, height, and contact angle vary radically for the two fluids. Picknett and Bexon [13] derived an expression for the evaporation rate based on the solution of the Laplace equation for the vapor concentration as a function of the contact angle. Hu and Larson [14] solved the evaporation problem in the absence of deposit formation numerically and Schönfeld et al. [15] found an approximate solution for the drop volume evolution for pinned drops. Popov [16] derived an analytical expression for the evaporation rate for arbitrary contact angles. Saada et al. [17] used numerical simulations to show the importance of the substrate dimensions and the buoyancy flow in the gas phase for the evaporation rate of the drops for substrate temperatures higher than the environment temperature. The thermal effects of the heat transfer in the substrate on the evaporation process was considered by Sobac and Brutin [18]. They showed that the importance of the substrate on the evaporation process increases with temperature. Lopes et al. [19] developed a numerical model for the transient heat conduction in a droplet, the substrate and the vapor diffusion in the gas phase. They reported that the local temperature distribution at the liquid-gas interface is governed be the transient heat transport. Sefiane and Bennacer [20] incorporated thermal effects of the substrate induced by evaporative cooling at the liquid-vapor interface into the correlation for the evaporation rate of pinned drops. Sodtke et al. [21] studied theoretically and numerically evaporating drops on heated substrates in a pure vapor atmosphere. No studies have been found considering deposit formation and associated varying wettability in the numerical simulation of the evaporation process.

The cited literature shows that surface temperatures and evaporation play a major role in fuel derived deposit formation. In this work, the main focus is to investigate experimentally the evolution of the apparent contact angle and the drop volume for single fuel drops during evaporation depending on the substrate temperature and the presence of deposit. The work is focused on the influence of deposits on wetting and evaporation and vice versa but not on the chemical reactions.

Furthermore, the dependence of the deposited mass as well as deposit shape and structure on the wall temperature are evaluated. The correlations for drop evaporation evolution found by previous authors are applied to evaporating hydrocarbons with deposit formation. The results are compared to the experimental data.

The rest of this paper is structured as follows: Firstly the experimental setup, measuring technique and test conditions are presented in Section 2. Section 3 gives an overview of the physico-mathematical model used. The experimental results regarding drop impingement, evaporation and deposit formation are summarized in Section 4 before they are compared to the model (Section 5). A discussion of the major findings can be found in Section 6. Finally, a summary and conclusion are given (Section 7).

2. Experiment

2.1. Test cell and equipment for repeatable drop evaporation experiments

The test cell (1) and the experimental equipment for the repeatable drop evaporation experiments are shown in Fig. 1. A temperature controlled, electrical heater (2) conducted to power supply 1 is used to heat the aluminium (AlMg3) substrate. The arithmetic average roughness for the substrates R_a is between 0.122 and 0.351 µm. Within the substrate a thin thermocouple is mounted to measure the temperature 0.5 mm below the surface. To reduce the heat losses from the substrate heater to the test cell and the environment, additional electrical heaters are placed in the test cell corners. A controllable syringe pump (3) is used to feed the injector needle with an outer diameter of 0.4 mm, which is positioned 3.4 mm above the substrate surface. Condensation on the side view windows and a change of the atmospheric composition due to evaporation are avoided by the application of a slight air flow (20 g h^{-1}) entering at the cell head. Numerical investigations of the isothermic flow field show no major influence of the flow on the substrate (see supplementary material). The maximum Rayleigh number in the investigated scenarios is $Ra = 1.15$. Additionally, the vapor transport in the gas phase under the influence of forced convection and diffusion was considered. The results show that the effect of forced convection on the vapor transport and, thus, on the drop evaporation process is negligible. A detailed description of the simulation can be found in the supplementary material. Thus, a still environment in the area close to the drop is assumed. The supply of fresh air is monitored with a coriolis flow meter (4) and set by a pressurestat.

Condensable reactants are collected inside a condenser (5) before the waste air is led to the filter system. The drop shape is detected with a CMOS monochrome camera.

2.2. Test conditions and methods

The experiments are conducted with the double aromatic hydrocarbon methylnaphthalene, $C_{11}H_{10}$, as the test fluid. Preliminary drop evaporation experiments with different fuels and hydrocarbons and with wall temperatures close to the saturation point of each test fluid have shown a higher deposit formation tendency for aromatic hydrocarbons and especially for the double aromatic hydrocarbon, $C_{11}H_{10}$ (in comparison with Fig. 2). The generated deposits are similar in morphology to real engine deposits formed by evaporation of fuel found on pistons and injector tips.

The experimental procedure is as follows: After preheating the substrate and the test cell, 500 single fluid drops are impinged on the substrate surface and evaporated. The time scale of the deposit formation process is much larger than the time scale of the individual drop evaporation. Therefore the deposit pattern, which is formed from an individual drop evaporation is negligible and a large number of drops is needed. The drop frequency f_{drop} is set to values ensuring that the next drop impinges the surface after the complete evaporation of the previous drop: $\Delta\tau_{drop} = 1/f_{drop} > \Delta\tau_{evap}$. The number of drops is calculated from the feed volume and the feed rate of the syringe pump with an estimated error of ±5 drops. The procedure is executed for five wall temperatures, where three temperatures are below saturation (180 °C, 200 °C, 220 °C), one temperature is close to the saturation of methylnaphthalene (240 °C) and one temperature is above the saturation point

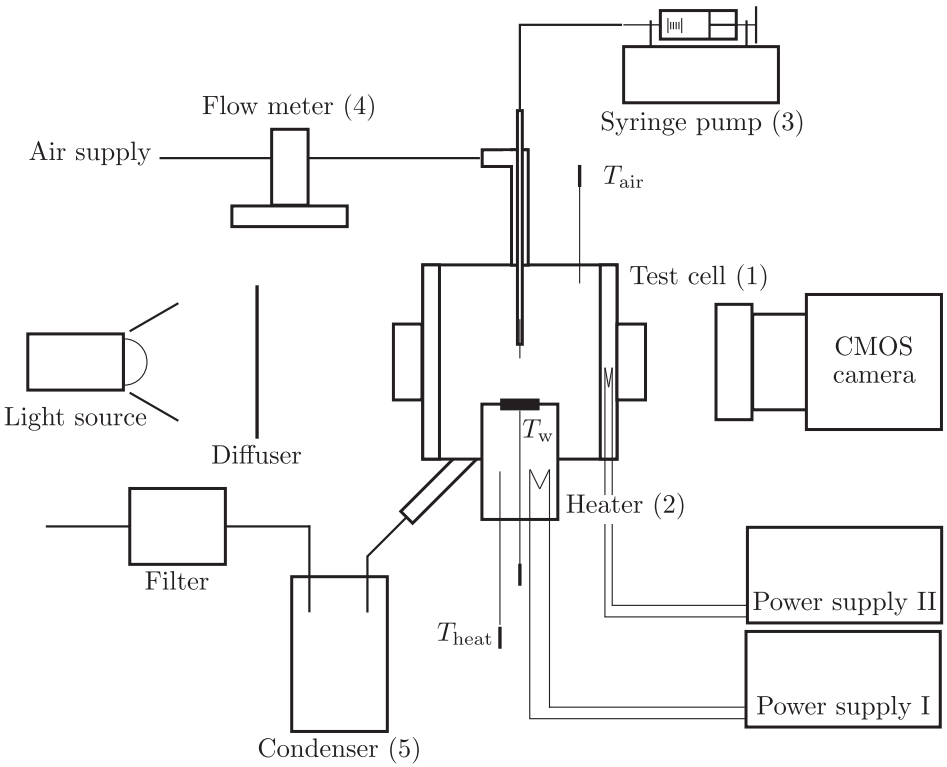

Fig. 1. Experimental setup for repeatable drop evaporation.

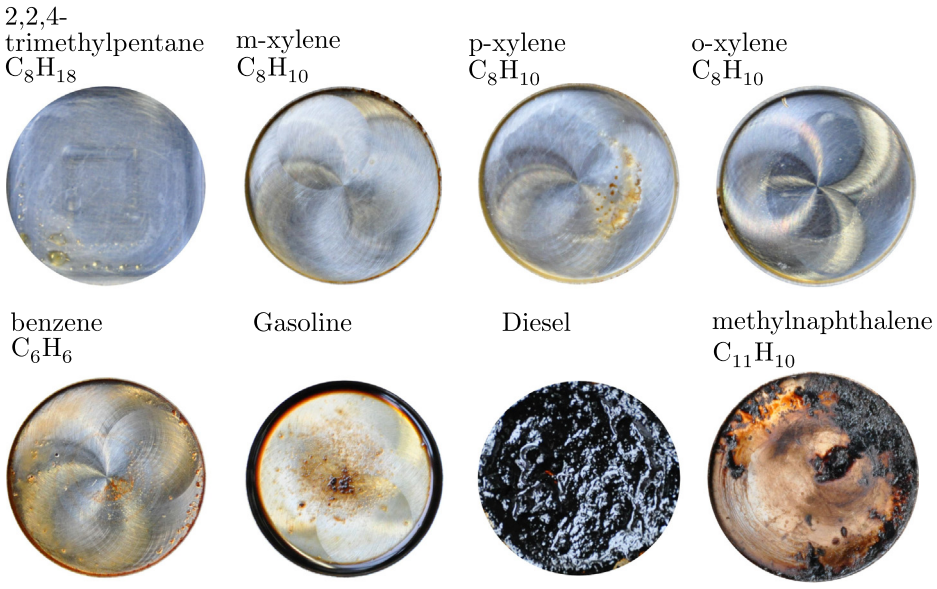

Fig. 2. Preliminary evaporation experiments with different types of hydrocarbons showing an increased deposit formation tendency for methylnaphthalene, $C_{11}H_{10}$.

(260 °C). During each experiment, the wall temperature is kept constant. The experimental conditions and the main fluid properties are given in Table 1. A CMOS monochrome camera is used to capture the side shadow image of the drop with a maximum frame rate of 380 frames/s. To ensure constant drop volumes, the diameter of the free falling drop is also recorded. With the installed camera system a spacial resolution of 8 µm/pixel is achieved. A Matlab-based code is used to binarize the camera recordings to obtain a sharp edged interface of the liquid phase and the surrounding air, Fig. 3 (a, b). Assuming the shape of a spherical cap, the apparent volume V_i at time i of the sessile drop can be calculated with

$$V_i = \frac{\pi}{6} h_i \left(\frac{3}{4} d_i^2 + h_i^2 \right), \tag{1}$$

where d_i is the spreading diameter and h_i the height of the sessile drop at the respective time. Since the Bond number Bo is approximately 0.29, the assumption that gravity can be neglected is justified. Both, the height h_i and the spreading diameter d_i are taken from a defined box surrounding the sessile drop. The apparent contact angle is evaluated by the following procedure: (I) Applying a convex hull to separate the liquid from the gas phase in the binarized image, Fig. 3(c). (II) Using the corner point of the surrounding

Table 1
Test conditions and fluid properties.

Parameter	Test 1	Test 2	Test 3	Test 4	Test 5
Substrate temperature (°C)	180	200	220	240	260
Air temperature (°C)	159	176	190	206	222
Air flow (g/h)	20	20	20	20	20
Drop volume (µl)	2.7	2.7	2.7	2.7	2.7
Drop diameter (mm)	1.6	1.6	1.6	1.6	1.6
Number of drops	500	500	500	500	500

Boiling point of 1-Methylnaphthalene: T_{sat} (1 bar) = 245 °C.
Fluid properties of liquid 1-Methylnaphthalene at 220 °C:
η_l = 0.56 mPa.s, σ = 20 mN/m, ρ_l = 864 kg/m^3, ρ_v = 3.47 kg/m^3, Δh_v = 338 J/g.

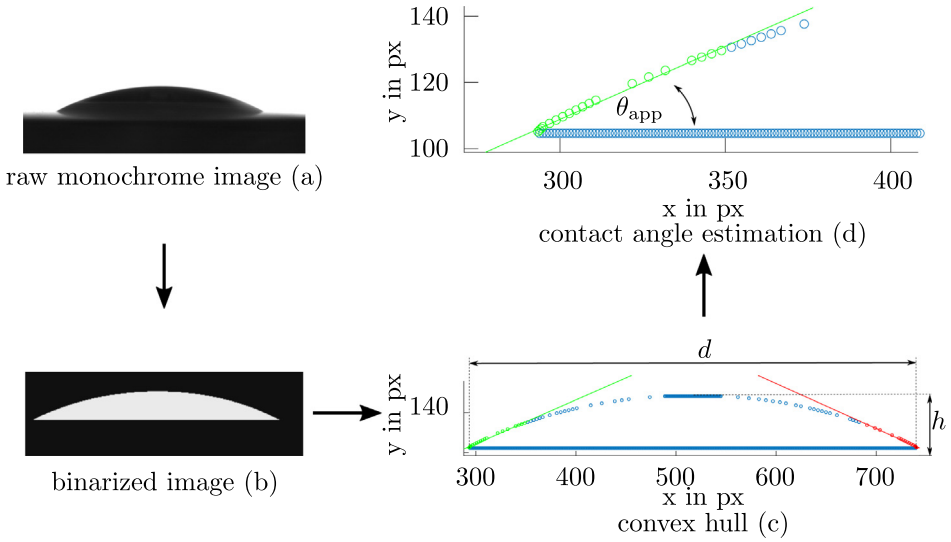

Fig. 3. Camera detection and post processing.

box and the subsequent vertices of the convex hull polygon to calculate a line of best fit. (III) The apparent contact angle is between the lower surface of the surrounding box and the line of best fit. With increasing number of vertices the calculated contact angles show a more regular trend leading however to an underestimation. Using only a small number of vertices produces high scattering. An optimal measure is to take all convex hull polygon vertices, that lie within 1/8 of the spreading diameter. In Fig. 3(d) a line of best fit is shown in company with the used polygon vertices. This procedure is applied to all drops and for each experiment. As the formation of deposits is not symmetrical, the data scattering increases for higher drop numbers. Therefore the data are manually filtered, taking only data sets with low scattering into account.

The deposit mass is evaluated from measurements with a precision scale (accuracy 1 mg). Before and after each experiment the substrate is weighed to calculate the deposit mass as the difference of clean and deposited substrate.

3. Physico-mathematical model

The physico-mathematical model considers an axi-symmetric, sessile drop evaporating in still air. The drop is small enough that the influence of gravity on the drop shape can be neglected. It can be assumed that the drop has the shape of a spherical cap. Picknett and Bexon [13] derived the evaporation rate of a drop formed like a spherical cap based on the solution of the stationary diffusion equation. The rate of change of the drop volume is given by:

$$\frac{dV}{dt} = -2\pi D[p_0(T) - p_\infty]\frac{M}{\rho_l R T}A(\theta), \tag{2}$$

with the drop volume V, time t, the diffusion coefficient of the vapor in air D, the molar mass M and density ρ_l of the liquid, universal gas constant R, temperature T, the far field partial pressure of the vapor p_∞ and the saturation vapor pressure at the interface $p_0(T)$. The function $A(\theta)$ depends on the contact angle θ and has been approximated by different correlations [13,14,20]. In this work the correlation for $A(\theta)$ obtained by Picknett and Bexon [13] as well as Hu and Larson [14] are used. Hu and Larson [14] solved the evaporation problem numerically to obtain an approximated equation valid for contact angles between 0° and 90°.

In Eq. (2) it is assumed that the drop interface has a uniform temperature T which is justified for thin drops sitting on a wall with constant temperature. Preliminary heat transfer simulations considering the drop on a heated aluminum wall of thickness 4 mm and incorporating evaporative cooling of the liquid-vapor interface have shown that the deviation of the interface temperature from the wall temperature ranges from 0.75 K for a wall temperature of 180 °C to below 3.5 K for 240 °C for the drops considered in the experiment. The resulting change in the governing pressure difference ranges from 2.2% to 7.5%. A more detailed description of the simulation setup can be found in the supplementary material. Therefore, in the following the wall temperature will be used in Eq. (2).

If the drop is pinned on the surface and the contact radius is constant, the evolution of volume with time can be computed by numerical integration of Eq. (2). However, Schönfeld et al. [15] derived an approximate analytical solution for the drop volume over time.

If, on the other hand, the drop is not pinned and the contact angle is constant, Eq. (2) can be directly integrated to obtain the

drop volume, as has been already shown by Picknett and Bexon [13].

In this work, the drops have been found to be evaporating in a stick-slide mode in the experiments. This means that the drop is initially pinned and the wetted area remains constant before a transition to a receding contact line with approximately constant contact angle can be observed. The measured drop diameter over time and the initial drop volume from the experiment are used as input parameters in the physico-mathematical model. The numerical scheme is structured as follows: from the experimentally measured diameter at a certain time instant and the calculated drop volume from the previous iteration, the drop height and contact angle are calculated using Eq. (1) and

$$\theta = 2\arctan(2h/d).$$

Eqs. (2) and (4) are used for the known geometry to compute the evaporation rate and consequently the volume change for the current iteration.

The volume change is determined using Eq. (2) with the correlation for $A(\theta)$ derived by Picknett and Bexon [13]

$$A(\theta) = f\left(\frac{3V}{\pi\beta}\right)^{1/3}, \tag{3}$$

with $\beta = (1-\cos\theta)^2(2+\cos\theta)$ and

$$f = 0.00008957 + 0.6333\,\theta + 0.116\,\theta^2 - 0.08878\,\theta^3 + 0.01033\,\theta^4 \quad \text{for} \quad \theta > 10^\circ$$

$$f = 0.6366\,\theta + 0.09591\,\theta^2 - 0.06144\,\theta^3 \quad \text{for} \quad \theta \leqslant 10^\circ$$

and Hu and Larson [14]

$$A(\theta) = 0.5(2.7\theta^2 + 1.30)\frac{d}{2}. \tag{4}$$

No significant difference between the two models was observed in the investigated scenarios.

Popov [16] derived an exact analytical expression for the evaporation rate independent of the contact angle. However, it has been shown that the easier expression by Hu and Larson captures the evaporative process very well for contact angles below 90° [22], which is why the model by Hu and Larson has been chosen in this work.

The model is implemented into the program MATLAB. The saturation vapor pressure $p_0(T)$ is calculated using a Wagner equation [23] and the temperature dependence of liquid density is accounted for. The diffusion coefficient is fit to the experimental data but kept constant for varying wall temperatures at $D = 2.3 \cdot 10^{-5}$ m²/s. For a comment on the evaluation of the diffusion rate, please see the supplementary material. The diffusion problem is quasisteady, since the characteristic diffusion time d^2/D, is much smaller than the characteristic evaporation time of a drop and the problem is diffusion-limited, which means that the interfacial resistance to evaporation is much smaller than the diffusion resistance to transport of vapor. Using this model it is possible to compare the volume, drop height and contact angle over time to the experimentally measured values. The model assumptions can be verified using the comparison between the experimental and model results.

4. Experimental results

4.1. Drop impingement and spreading

Fig. 4(a) shows the drops shortly before impingement on the clean substrate for the different wall temperatures. It has been confirmed by image analysis, that the initial drop volume is approximately constant for all experiments. After the impingement with a low velocity, the drops spread on the substrate surface showing some oscillations. Neglecting the gas temperature difference between needle tip and substrate surface and assuming constant liquid temperature of the falling drop, the Weber number is estimated to be in the order of 4–5. The maximum spreading diameter is reached with the first forward motion of the sessile drop (Fig. 4(b)). The data evaluation is started after the drop oscillation decayed. Thus, the sessile situation is assumed. The time instant zero corresponds to the moment when the drop oscillations have decayed. From Figs. 4(c) and 5 it can be seen, that for wall temperatures T_w = 220 °C and higher, an increasing wall temperature results in a decreased spreading diameter, whereas the drop height increases. In Fig. 6 the images with the maximum spreading diameters for the 10th, 100th and 500th drop and the images with the time after complete evaporation of the 500th drop are shown for the different wall temperatures. With an increasing number of evaporated drops, deposits are formed on the substrate surface.

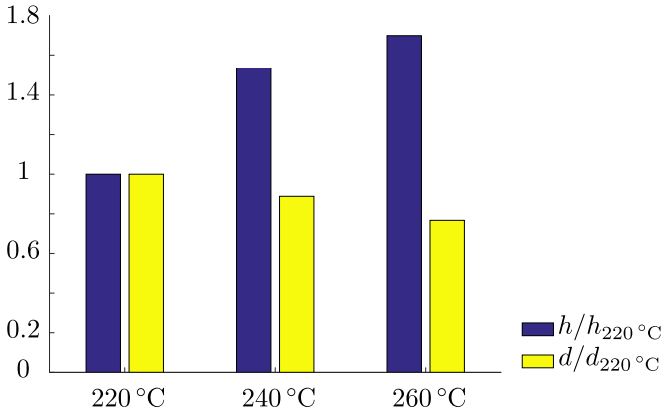

Fig. 5. Initial drop height and drop diameter.

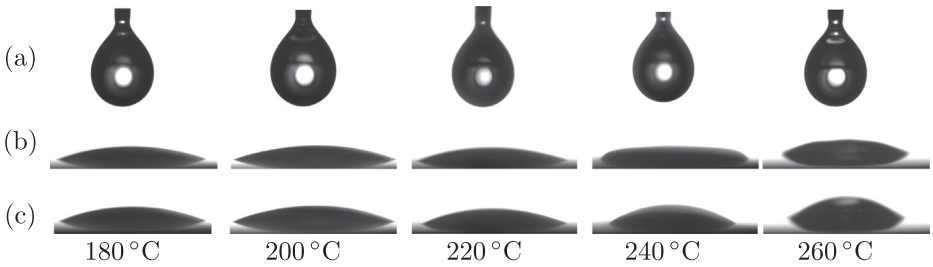

Fig. 4. Raw images of drops at the injector tip shortly before impingement (a), maximum spreading diameter during impingement (b) and stable drop shape after impingement (c) for different substrate temperatures on clean substrate.

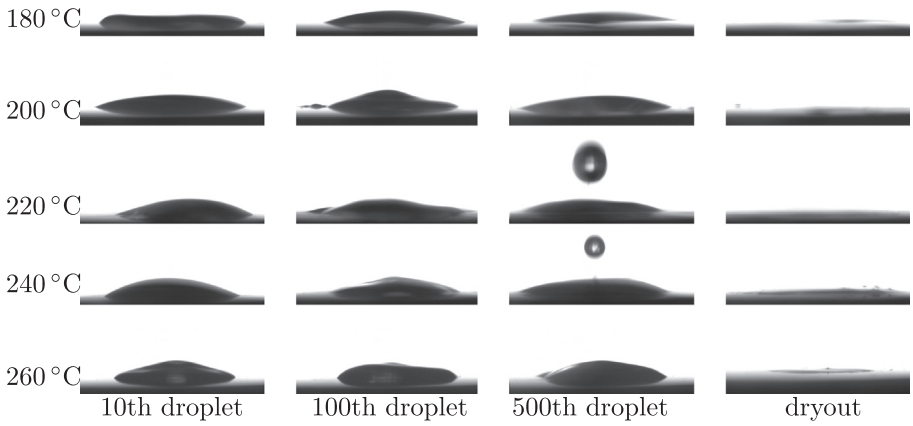

Fig. 6. Raw images of the sessile drops with its maximum spreading diameter for different substrate temperatures: 10th drop, 100th drop, 500th drop.

Detecting the drop's geometry becomes challenging when deposit particles adhere on the substrate and liquid remainings imbibed in the porous deposit structure, which is not completely evaporated and interact with the impinging drops. This can be seen in the cases for $T_w = 220\,°C$ and $T_w = 240\,°C$, where secondary drops are formed during the drop spreading. The liquid-solid interface gets unclear and disordered, which leads to higher apparent drop volumes, although the drop generator creates drops with constant volumes. Two main observations for the drop spreading on the surface covered by deposits can be made. One is that the deposits lead to a non-uniform spreading of the liquid phase after impingement. The second observation is that the wall deposits reduce oscillations during the spreading.

4.2. Evaporation

The apparent contact angle and the drop volume are analyzed to evaluate the evaporation behavior of the fuel drops. Fig. 7 shows the time-dependent apparent contact angle θ_{app} for the first drop impinging on the clean substrate surface for various surface temperatures. In this situation the drop evaporation is described by a stick-slide mode, meaning that the drop is initially pinned and transitions to a constant contact angle mode [24]. With increasing time the contact angle θ_{app} decreases until a threshold of approx. 15° is reached and then remains almost constant until the drop is completely evaporated. The data scattering increases for small drop sizes as reflection becomes more prominent and impedes the drop detection. At ambient conditions with $T_w = 22\,°C$ in still air and for a clean substrate, an initial contact angle of 6.5 ± 1.5 degree has been measured. It has been observed that for higher wall temperatures the initial apparent contact angle increases. This tendency is confirmed by a lower maximum spreading diameter and a larger drop height (Fig. 8(a)). Above the saturation point the data scattering increases and boiling occurs. In some cases the single drop does not contact the substrate, but rather levitates in its own vapor layer, which can be referred to the Leidenfrost effect.

The volume over time plots in Fig. 8(b) show the decreasing drop lifetime for higher surface temperatures on the clean substrates. Thus, the global evaporation increases.

4.3. Deposit formation

The results of the deposit formation are listed in Table 2, containing the pictures of the substrates taken after the experiment. A clean substrate is shown for reference. For $T_w = 180\,°C$ noticeable dark yellow to light brown deposits with small dark brown particles were formed close to the edge of the substrate surface.

In the experiments with higher wall temperatures a remarkable deposit formation can be seen not only at the edge of the substrate surface but also closer to the substrate center. However, in the very center, at the location of the drop impingement, no deposit formation can be observed. For $T_w = 220\,°C$ the deposit layer becomes darker and includes dark brown deposit particles. The highest deposition mass has been observed for the experiments close to the saturation point. A substrate surface temperature of $T_w = 240\,°C$ leads to a dark brown to black deposit layer in the center of the substrate surface. It is noticeable that close to the edge of

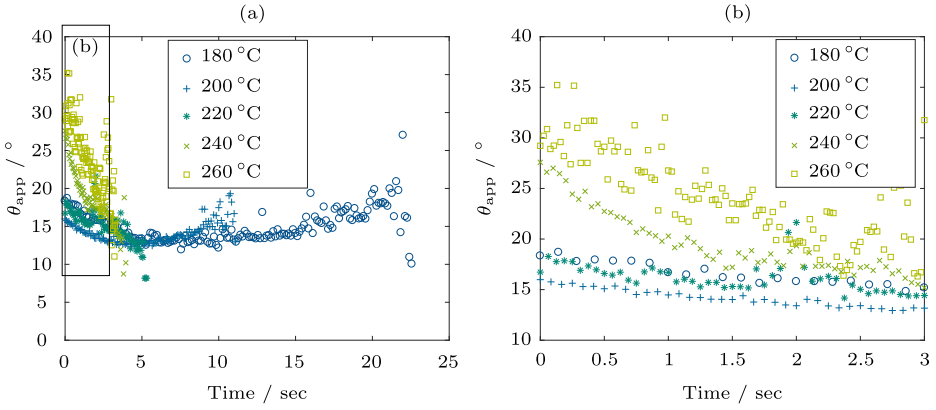

Fig. 7. Apparent contact angle for the first drop on the clean substrate surfaces for increasing wall temperatures: (a) entire drop evaporation, (b) evaporation process from 0 to 3 s.

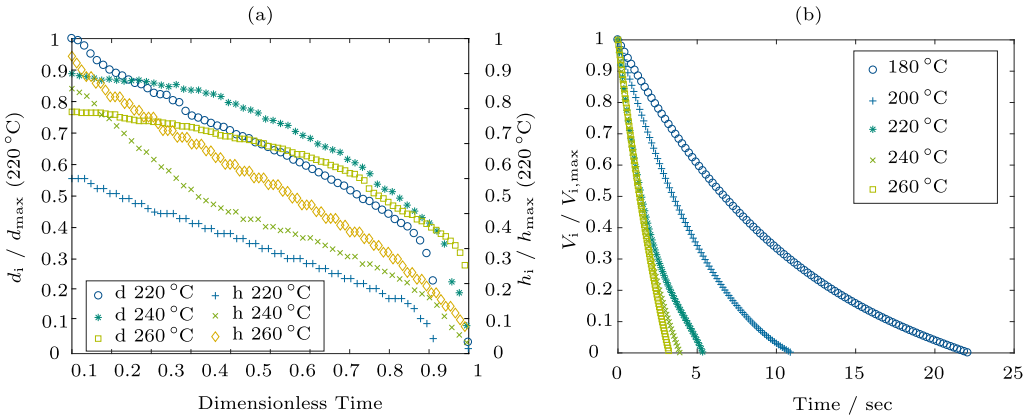

Fig. 8. Maximum drop spreading diameter and drop height over dimensionless time, defined in relation to drop life time (a), fitted drop volume over time (b) for the initial drops on the clean surface.

Table 2
Deposit formation after each drop test for varying wall temperatures.

Wall temperature	180 °C	200 °C	220 °C	240 °C	260 °C
Deposited mass	2 mg	4 mg	5 mg	8 mg	2 mg

the substrate surface no prominent deposit formation has taken place during this experiment. In the experiments with surface temperatures above the saturation point, the deposited area is even smaller, and the final deposition mass was much lower.

The deposit layers for $T_w = 240$ °C and $T_w = 260$ °C have been analyzed with a 3D confocal microscope and showed similar characteristics. From the images of Fig. 9 it can be seen that the layer has an average thickness of 20–30 µm with some higher peaks. The solid deposit layer has an irregular mesh-like surface morphology including pores of different sizes.

The evolution of the contact angle over time for the experiments at $T_w = 240$ °C at different stages of deposit formation in Fig. 10(a), shows a direct influence of the deposit formation on the evaporation regime close to the saturation point.

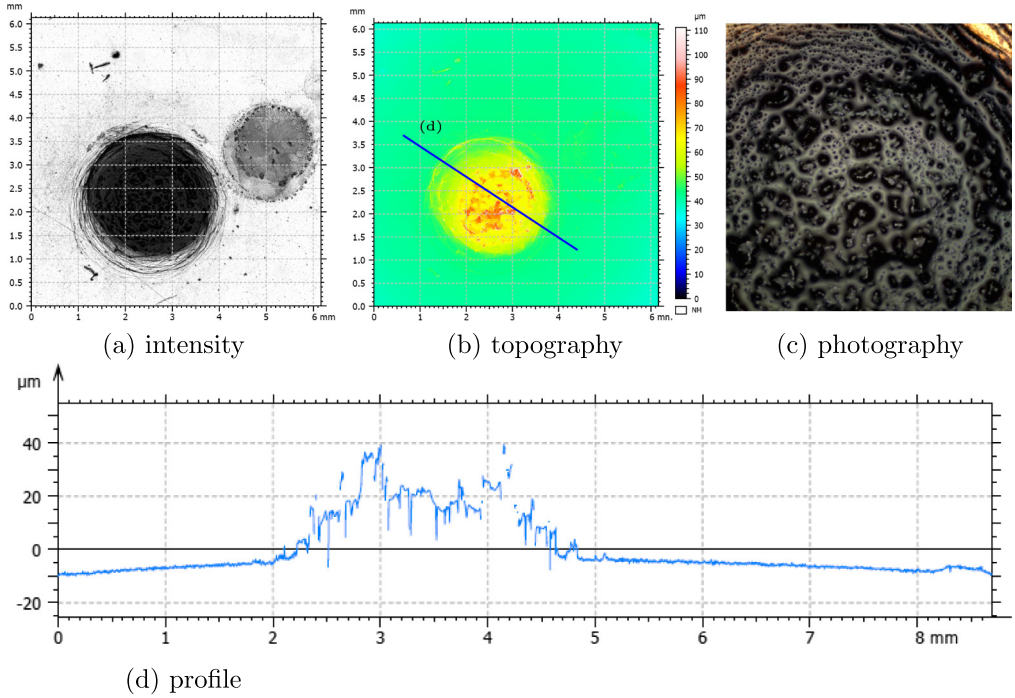

Fig. 9. 3D confocal microscope analysis of deposit layer for $T_w = 260$ °C.

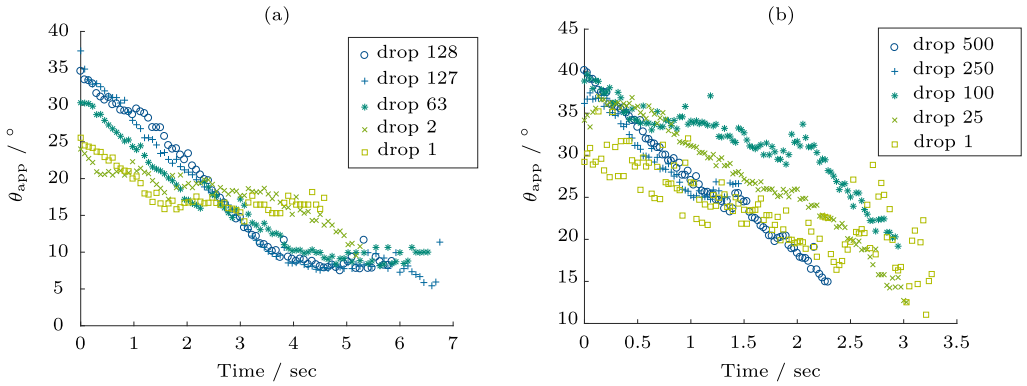

Fig. 10. Apparent contact angle measurements for T_w = 240 °C (a) and T_w = 260 °C (b).

With an increasing deposit layer the pinning of the drop gets more prominent. As the deposit layer growths, a sharp decrease of contact angle evolution is observed, indicating the pinning regime.

However, for the experiment above the saturation point at T_w = 260 °C the contact angles decrease slowly with time. The contact angle evolution does not change significantly from droplet to droplet. Thus, the deposit formation does not have a major influence on the wetting behavior during the detected time frame.

5. Model results

The drop volume over time plots from the experimental data for the first drop and the model calculations are shown in Fig. 11(a). As one can see, the numerical results agree with the experimental data very well. Only small derivations between the experimental and numerical results can be observed for T_w = 200 °C. The evaporation time is predicted very well in both cases. A line showing the linear decrease of $V^{2/3}$ with time (constant contact angle model [13]) is included in Fig. 11(a) to demonstrate that the evaporation process can be described using this relation (compare Fig. 12). This is possible, since the influence of the contact angle on the evaporation rate is not strong.

Fig. 11(b) shows the result of the drop height obtained in the experiment for the first drop and the model computations. Although the agreement between the numerical and experimental results is good, the derivations are higher than between the experimentally and numerically obtained evolution of drop volume. The drop shape detection becomes more difficult in the experimental setup with decreasing drop size so that the derivations could be attributed to measurement uncertainties.

The obtained contact angle values of the model are compared to the experimental data for the first drop in Fig. 12. The contact angles from the physico-mathematical and the experimental investigations agree very well. In the case of T_w = 200 °C the numerically obtained contact angles are a little higher than the measured apparent contact angles. However, the physico-mathematical simulations lead to a much smoother plot of the contact angle. This means that the model can be used to complement the experimentally obtained contact angles to achieve more accurate data. For T_w = 200 °C and 240 °C the contact angle remains almost constant throughout the evaporation process after the short initial linear decrease. This explains the good agreement with the $V^{-2/3}$ line in Fig. 11(a) as this is the expected shape for a drop evaporating in still air with a constant contact angle (compare [13,15]). This result could not be gained by looking at the experimentally measured contact angle data alone, as a noticeable scatter in the data does not allow the conclusion that the constant angle remains constant.

6. Discussion

6.1. Contact angle

The experimental results show the difficulty in analyzing the drop evaporation for deposit building fuels, since the deposit formation process is strongly interrelated with the wetting of the substrate and with the heat transport and phase change processes of the sessile drop. For clean substrate surfaces the apparent contact

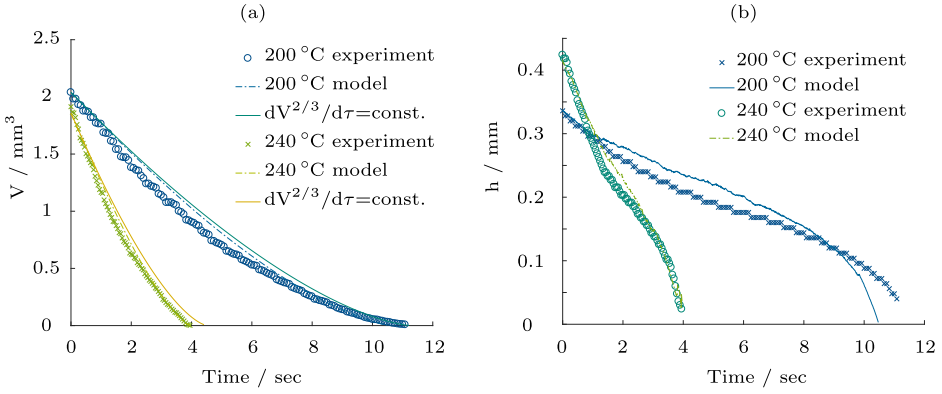

Fig. 11. (a) Drop volume over time for the initial drop in experiment and physico-mathematical model for different temperatures. (b) Drop height over time for the initial drop in experiment and physico-mathematical model for different temperatures.

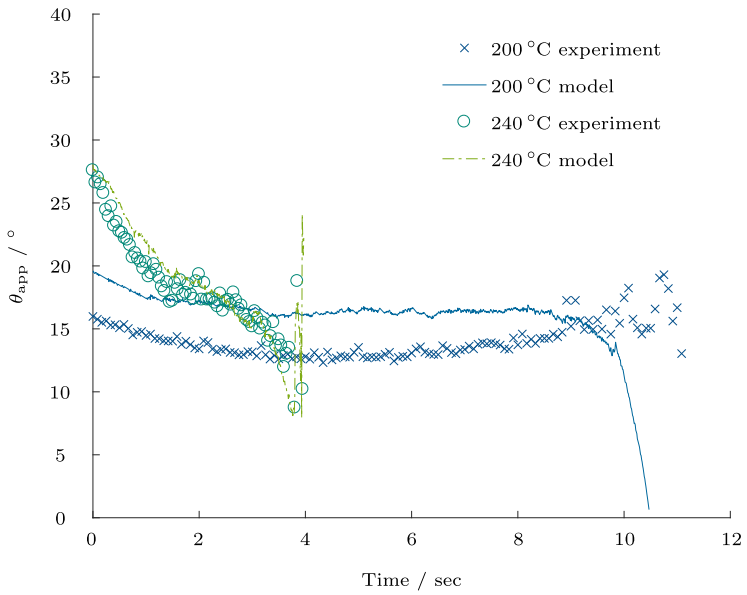

Fig. 12. Contact angle over time for the initial drop in experiment and physico-mathematical model for different temperatures.

angle increases for higher surface temperatures, which is in line with the study of Raj et al. [25], where the authors observed a linear increase of the contact angle of an FC-72 sessile drop for increasing wall superheats. With increasing wall superheat, the evaporation in the vicinity of the three-phase contact line is enhanced and requires a higher liquid flow from the drop bulk to the contact line. This higher liquid flow is enabled by an increased pressure drop, which is coupled with a higher curvature gradient and, thus, with the higher contact angle. In the experiments presented in the present work, higher evaporative mass flows occur for higher wall and gas temperatures, since the vapor saturation concentration, which is coupled with the saturation vapor pressure, increases.

The wetting characteristics change with increasing order number of drops as the deposit formation changes the substrate surface topography and its roughness. Kandiklar and Steinke observed a direct influence of the latter on the contact angle [26]. With increasing surface roughness, the apparent contact angle first decreases but then starts increasing again. The authors suggested that higher roughness structures interfere with the spreading behavior and increase the contact angle. Bico et al. [27] concluded that higher contact angles occur for drops in the pure Wenzel regime, which might take place in the present case for the evaporating drop on the deposited substrate surface.

As shown in the experimental results, the movement of the three phase contact line on the clean substrate surface during evaporation transitions from constant contact diameter to approximately constant contact angle. The pinning forces due to chemical and geometrical heterogeneities keep the contact line in position but with a stronger flattening of the spherical cap during evaporation, the depinning-forces grow and finally lead to depinning [28]. In the presence of solid deposit layers or deposit particles the geometrical heterogeneities increase and the pinning phases become longer, which has been observed in the experiment.

6.2. Deposit formation

In the pictures in Table 2 two different deposit formation tendencies can be observed. Substrate temperatures below the saturation point lead to an irregular deposit formation close to the substrate surface edge, while the substrate center remains almost clean. The presence of deposits in the edge region leads to the assumption that chemically formed deposit precursors are transported to the pinning contact line comparable to the coffee-ring effect [29]. However, the deposition band contains a highly viscous film, which is rather broad and has an undefined and smooth transition to the clean substrate center. The entire substrate surface is deposited and the maximum spreading diameter of each sessile drop is less than one third of the substrate diameter. It is likely, that the chemically formed deposit layer contains only precursors, which did not evaporate and which were not able to form solid deposits. The successively falling drops wash the precursors away from the center in the edge region, where they agglomerate.

For substrate temperatures close to and above the saturation point, the deposit formation is more intense and concentrated to the substrate center. A typical coffee-ring stain can been observed, which is overlapped by a dense dark brown to black deposit layer. We assume that deposit particles were chemically formed inside the drop and transported to the pinning contact line. This process could be superimposed by an unstructured agglomeration of deposit particles on the substrate surface inside the drop. Hu et al. [30] and Yunker et al. [31] reported possible mechanisms for this deposition phenomenon. Assuming Marangoni flow inside the drop, the coffee-ring effect can be reversed and deposit particles are more likely to adhere in the substrate center. Yunker et al. used ellipsoids in drying liquid drops and observed a uniform deposit pattern on the substrate [31]. Those anisotropic particles showed strong bounds, which resisted the radial outward flow.

Another possible reason for the solid deposit pattern is the non-pinning phase at the end of the evaporation process. As the spreading radius decreases, deposit particles are pulled together and build deposit patterns, which adhere to the wall. Despite the significantly shorter drop lifetime for the higher substrate surface temperatures, the deposition mass increases until the saturation point, which underlines the major effect of wall temperature on the deposit formation process. This is also supported by the observations for the experiment with $T_w = 260\,^{\circ}C$, where the drop lifetime is almost identical as in the experiment with $T_w = 240\,^{\circ}C$ but the deposition mass significantly decreases.

It has been shown by comparing the physico-mathematical results to the experimental values that the drop evaporation is driven by an effective vapor diffusion in the gas phase and that the assumption of spherical drops holds as long as the deposit structure does not interfere with the wetting behavior. The results of the

model can be used to identify the change of contact angle over time. A stick-slide mode behavior is observed. The contact angle remains almost constant for higher times for some drops and the volume change is in line with the predictions for a non-depositing liquid. Though the deposit formation of a single drop seems to be negligible, a long term influence of the deposit formation on wetting is obvious. Conclusively, the drop evaporation on deposited surfaces will differ significantly from that on clean surfaces.

7. Summary & conclusion

In the presented work the drop shape evolution, the apparent contact angle and the lifetime of methylnaphthalene drops have been measured experimentally for varying wall temperatures to investigate the hydrodynamics, the evaporation and the deposit formation tendency of liquid hydrocarbons. Existing correlations have been applied for the prediction of evaporation rates. The drop evaporation can be described using an effective diffusive vapor transport.

The experimental data show a major effect of wall temperature on the deposit formation. The observed deposits vary from dark yellow and light brown viscous films for wall temperatures 25 K below saturation point to dark brown and black solid deposits for wall temperatures close to and above saturation temperature. Though the detailed chemistry of methylnaphthalene deposit formation is not known, two main conclusions can be drawn: First, at temperatures 25 K below saturation point, the formation process leads to soluble deposit precursors, which can be washed away by subsequent drop impacts. Second, polymerization and chemical condensation reactions, which lead to insoluble macromolecules appearing as solid deposits, take place at temperatures close to and above saturation point. The wall temperature also has a direct influence on the drop shape evolution. With increasing wall temperature, the spreading diameter reduces, drop height and apparent contact angle increase. This reduced wetting comes along with a shorter drop lifetime. The latter one is a consequence of enhanced evaporation. The experiments emphasized the complexity of deposit formation of hydrocarbon based fuel components. As the wall temperature influences both, the deposit formation and the wetting characteristics, it is the most prominent parameter in this work. Solid deposits increase the surface heterogeneities and increase the drop pinning phase duration during evaporation.

Conflict of interest

The authors declared that there is no conflict of interest.

Acknowledgements

The authors would like to thank the German Research Foundation DFG for their financial support within the Collaborative Research Centre SFB/TRR 150 “Turbulent, chemical reactive near-wall multiphase flows”, subprojects A01 & B01.

Appendix A. Supplementary material

Supplementary data associated with this article can be found, in the online version, at https://doi.org/10.1016/j.ijheatmasstransfer.2018.08.102.

References

[1] D.C. Arters, M.J. Macduff, The effect on vehicle performance of injector deposits in a direct injection gasoline engine, SAE (2000-01-2021), 2000.
[2] D.C. Arters, E.A. Bardasz, E.A. Schiferl, D.W. Fisher, A comparison of gasoline direct injection and port fuel injection vehicles; part i – fuel system deposits and vehicle performance, SAE, 1999.
[3] O. Güralp, M. Hoffmann, D. Assanis, Z. Filipi, T.-W. Kuo, P. Najt, R. Rask, Characterizing the effect of combustion chamber deposits on a gasoline hcci engine, SAE (2006-01-3277), 2006.
[4] M. Kinoshita, A. Saito, S. Masushita, H. Shibata, Y. Niwa, A method for supressing formation of deposits on fuel injector for direct injection gasoline engine, SAE (Vol 108 Part 4), 1999, pp. 2177–2184.
[5] T. Ashida, Y. Takei, H. Hosi, Effects of fuel properties on sidi fuel injector deposit, SAE (2001-01-3694), 2001.
[6] B. Richter, S. Crusius, U. Schümann, H. Harndorf, Charakterisierung interner ablagerungen in common-rail-injektoren, MTZ - Motortechn. Z. 74 (10) (2013) 796–803.
[7] H. Song, J. Xiao, Y. Chen, Z. Huang, The effects of deposits on spray behaviors of a gasoline direct injector, Fuel 180 (2016) 506–513.
[8] Y.M. Arifin, T. Furuhata, M. Saito, M. Arai, Diesel and bio-diesel fuel deposits on a hot surface, Fuel 87 (8–9) (2008) 1601–1609.
[9] Y.M. Arifin, M. Arai, Deposition characteristics of diesel and bio-diesel fuels, Fuel 88 (11) (2009) 2163–2170.
[10] Robert D. Deegan, Olgica Bakajin, Todd F. Dupont, Greb Huber, Sidney R. Nagel, Thomas A. Witten, Capillary flow as the cause of ring stains from dried liquid drops, Nature 389 (6653) (1997) 827–829.
[11] J. Schmid, I. Zarikos, A. Terzis, N. Roth, B. Weigand, Crystallization of urea from an evaporative aqueous solution sessile droplet at sub-boiling temperatures and surfaces with different wettability, Exp. Therm. Fluid Sci. 91 (2018) 80–88.
[12] Elyssa F. Crafton, W.Z. Black, Heat transfer and evaporation rates of small liquid droplets on heated horizontal surfaces, Int. J. Heat Mass Transfer 47 (6) (2004) 1187–1200, https://doi.org/10.1016/j.ijheatmasstransfer.2003.09.006, ISSN 0017-9310.
[13] P.G. Picknett, R. Bexon, The evaporation of sessile or pendant drops in still air, J. Colloid Interface Sci. 61 (2) (1977) 336–350, https://doi.org/10.1016/0021-9797(77)90396-4.
[14] H. Hu, R.G. Larson, Evaporation of a sessile droplet on a substrate, J. Phys. Chem. B 106 (6) (2002) 1334–1344, https://doi.org/10.1021/jp0118322.
[15] F. Schönfeld, K.-H. Graf, S. Hardt, H.-J. Butt, Evaporation dynamics of sessile liquid drops in still air with constant contact radius, Int. J. Heat Mass Transfer 51 (13–14) (2008) 3696–3699, https://doi.org/10.1016/j.ijheatmasstransfer.2007.12.027.
[16] Yuri O. Popov, Evaporative deposition patterns: spatial dimensions of the deposit, Phys. Rev. E 71 (2005) 036313, https://doi.org/10.1103/physreve.71.036313.
[17] Mebrouk Ait Saada, Salah Chikh, Lounès Tadrist, Numerical investigation of heat and mass transfer of an evaporating sessile drop on a horizontal surface, Phys. Fluids 22 (11) (2010) 112115, https://doi.org/10.1063/1.3488676.
[18] B. Sobac, D. Brutin, Thermal effects of the substrate on water droplet evaporation, Phys. Rev. E 86 (2012) 021602, https://doi.org/10.1103/PhysRevE.86.021602.
[19] M.C. Lopes, E. Bonaccurso, T. Gambaryan-Roisman, P. Stephan, Influence of the substrate thermal properties on sessile droplet evaporation: effect of transient heat transport, Colloids Surfaces A: Physicochem. Eng. Aspects 432 (2013) 64–70.
[20] K. Sefiane, R. Bennacer, An expression for droplet evaporation incorporating thermal effects, J. Fluid Mech. 667 (2011) 260–271, https://doi.org/10.1017/s0022112010005446.
[21] Christof Sodtke, Vladimir S. Ajaev, Peter Stephan, Dynamics of volatile liquid droplets on heated surfaces: theory versus experiment, J. Fluid Mech. 610 (2008) 343–362, https://doi.org/10.1017/S0022112008002759.
[22] B. Sobac, D. Brutin, Triple-line behavior and wettability controlled by nanocoated substrates: influence on sessile drop evaporation, Langmuir 27 (24) (2011) 14999–15007, https://doi.org/10.1021/la203681j.
[23] B.E. Poling, J.N. Prausnitz, J.P. O'Connel, The Properties of Gases and Liquids, fifth ed., McGrawHill, 2001.
[24] J.M. Stauber, S.K. Wilson, B.R. Duffy, K. Sefiane, On the lifetimes of evaporating droplets, J. Fluid Mech. (2014) 744, https://doi.org/10.1017/jfm.2014.94, ISSN 0022-1120.
[25] R. Raj, C. Kunkelmann, P. Stephan, J. Plawsky, J. Kim, Contact line behavior for a highly wetting fluid under superheated conditions, Int. J. Heat Mass Transfer 55 (9–10) (2012) 2664–2675.
[26] S.G. Kandlikar, M.E. Steinke, Contact angles and interface behavior during rapid evaporation of liquid on a heated surface, Int. J. Heat Mass Transfer 45 (2002) 3771–3780.
[27] J. Bico, C. Tordeux, C. Quéré, Rough wetting, Europhys. Lett. 55 (2001) 214–220.
[28] D. Orejon, K. Sefiane, M.E.R. Shanahan, Stick-slip of evaporating droplets: substrate hydrophobicity and nanoparticle concentration, Langmuir: ACS J. Surfaces Colloids 27 (21) (2011) 12834–12843.
[29] R.D. Deegan, O. Bakajin, T.F. Dupont, G. Huber, S.R. Nagel, T.A. Witten, Contact line deposits in an evaporating drop, Phys. Rev. E 62 (1) (2000) 756–765.
[30] H. Hu, R.G. Larson, Marangoni effect reverses coffee-ring depositions, J. Phys. Chem. B 110 (14) (2006) 7090–7094.
[31] P.J. Yunker, T. Still, M.A. Lohr, A.G. Yodh, Suppression of the coffee-ring effect by shape-dependent capillary interactions, Nature 476 (7360) (2011) 308–311.